Target Localization by Mobile Handheld UHF RFID Reader and IMU

Aristidis Raptopoulos Chatzistefanou, Anastasios Tzitzis, Spyros Megalou, George Sergiadis, *Member, IEEE,* Antonis G. Dimitriou, *Senior, IEEE*

Abstract—In this paper we design and construct a mobile handheld human operated device used to guide the user towards the desired RFID-tagged target, and at the same time provide estimations of the distance and the angle from the user to the target. The main components of the device are a UHF RFID reader operating with one antenna and an Inertial Measurement Unit (IMU), used to measure rotation angles. During the movement of the operator, phase of arrival and rotation angle data are collected by the RFID reader and the IMU respectively. A particle filter algorithm leverages the collected data to estimate the distance and angle of the operator, with respect to his/her current pose. As more iterations are completed, the fusion of multiple measurements improves the estimation performance. Experimental results show a mean angle estimation error of $\sim 6^o$, and distance estimation error less than $0.5m$ when the user approaches the target after few iterations. Recorded computational time is small-enough to enable real time tracking-applications.

Index Terms—RFID, portable, phase, localization, tracking.

I. Introduction

Radio Frequency Identification (RFID) technology's penetration in health care, logistics, and security market has been rapid in the last decade. Innovative RFID applications begin to emerge in various fields, aiming to provide services like assisted living, or enhanced and personalised user related experiences.

In this paper, we propose and construct a handheld UHF RFID reader, capable to guide the user towards a specific tag. The proposed device uses RFID technology to estimate the location of the target RFID tag relative to the user's pose. The prototype is developed in the context of project "CultureID", where we install UHF RFID technology inside the Archaeological Museum of Thessaloniki, Greece. An RFID tag is assigned to every exhibit. The proposed reader will be used as a "tool" in the context of games, developed for younger visitors inside the museum, guiding the visitors to the proper exhibit, to discover a hint related to a riddle, according to the game's script. However, the proposed device can be widely adopted for locating misplaced items in retail; a process currently being carried out by increasing/decreasing the sound of a beeper from a handheld reader, depending on the measured backscattered power.

Prior art consists of works in which data are collected by a mobile agent; either *i)* a mobile robot equipped with the measuring device(s), or *ii)* a human holding the device(s). The collected data are used to estimate the position of the target in a way that its relative position to the position of mobile agent can be extracted. Data from other sources can also be fused with the measurements of the mobile agent to calculate its position.

Target localization with RFID technology includes works leveraging different aspects of the received signal information. The target is one or more stationary RFID tags. The measuring devices are mainly an RFID reader and a different number of antennas. Authors of [1] - [3] use the received signal power, or Received Signal Strength Indicator (RSSI). In [1] and [2], a mobile cart equipped with multiple antennas is moved in an area with scattered reference RFID tags at known locations. Both the cart's and target's position are calculated using RSSI measurements from the reference tags. In [3], a robot carries the measuring equipment. It creates a map of the experiment area, moves autonomously, and estimates its position on the map. A Bayesian filter and RSSI measurements are used to estimate the position of the target on the map.

RSSI measurements are highly ambiguous. Phase of Arrival (POA) measurements of the backscattered field are considered a more reliable alternative. POA however "suffers" from the 2π ambiguity. This can be avoided, by unwrapping the phase measurements, which requires sufficiently high read rate of the target RFID tag. In [4], wrapped phase measurements from two antennas on Simultaneous Localization And Mapping (SLAM) robot are used to locate the target tag. In [5] - [7], the authors achieve accurate 3D localization using unwrapped POA measurement. Multiple antennas are mounted on a robot performing SLAM. Given the robot's poses and the POA measurements, the optimal target position is calculated. A similar method is presented in [8], in which the robot's pose is calculated by a calibrated vision-based system. A mobile robot in [9] communicates in multiple frequency channels with the target RFID tag, to compensate for multipath effects, and locate the target. Authors in [10] propose a method to calculate the distance and bearing of the target tag relative to the robot's current pose, by using an Extended Kalman Filter (EKF) to fuse POA and odometry measurements. The robot tries to reach the target, and as it moves towards the estimated position, new measurements improve the estimation. In [11], handheld measuring system is implemented. The human operator's position is calculated using IMU measurements and phase measurements are collected in order to locate targets

in a multipath rich environment. In [12] POA measurements are collected by a custom Multiple-Input Multiple-Output (MIMO) antenna built, carried around by a robot. A Particle Filter (PF) algorithm is used to estimate the target's position. Authors in [13] also leverage PFs, but their robot utilizes Commercial Off The Shelf (COTS) RFID equipment. In [14], the position of the target tag is calculated using Particle Swarm Optimization (PSO). In [15] - [16], the mobile agent is a drone with RFID equipment, and both RSSI and POA measurements are utilized to locate the target.

Apart from RFID technology, guiding and navigation is also achieved by other means. In [17], a study about indoor positioning technologies is conducted. Among the practices presented are vision-based systems, infrared radiation, ultrasound localization, other RF technologies such as Wi-Fi and bluetooth and inertial navigation systems. In [18], a device, consisting of a camera, a Wi-Fi sensor and an IMU, is used to create a 3D map of the environment and afterwards locate the human operator in this map. In [19] - [21], camera and smartphone/tablet inertial sensors create the map, and an Augmented Reality (AR) application is navigating the user to the desired location, providing optical or auditory directions.

In this paper, we propose a novel method for RFID localization using a handheld human operated device. The device consists of a COTS RFID reader and an IMU. The user is instructed by the device to perform certain motions during which RFID reader and IMU measurements are collected. The proposed method leverages the collected data to provide the user with an estimation of the distance and angle of a desired RFID tag. The contribution of the proposed method can be summed up as follows:

- The proposed device consists of COTS RFID equipment, and is carriable by a human operator.
- The moving agent is a human, carrying the device.
- No previous knowledge of the search area is required, e.g. a map of the environment produced by SLAM or computer vision, or a reference RFID tag grid.
- All the required data are collected by the device and are locally processed to compute localization results.
- All of the above grant our method easy application in various scenarios.

In section II, the proposed method is described. Conducted experiments and their results are presented in section III. Finally, in section IV, conclusions and future work is discussed.

II. Proposed Method

In this paper we aim to improve our older work presented in [22]. The proposed method leverages measurements from a handheld device, operated by a human user, and guides the user to the desired RFID tag. The handheld device consists of two main components:

- An RFID reader, communicating with the target RFID tag.
- A 9 Degrees of Freedom IMU (9DoF IMU), measuring the rotation angle of the device.

The RFID reader is connected to one antenna, whose main radiating lobe is parallel to the ground. The IMU is placed

in such way to measure the rotation angle of the device on a plane parallel to the ground. A prototype of the described device can be seen in Fig. 1. The user is instructed by the device to execute three types of "commands":

- SCAN command: The user is requested to move the device on a circular trajectory parallel the ground, "scanning" the area in front of the user. Such a motion can be achieved, if the user "sticks" the upper part of the arm (from the shoulder to the elbow) to the torso, and rotates the rest of the arm (from the elbow to the hand) around the elbow, keeping it parallel to the ground. As the user moves the device, received signal phase measurements are collected by the RFID reader, and rotation angle measurements by the IMU. The collected data is used to estimate the distance and direction of the target tag with regard to the current user's pose. An illustration of the top view of the user and the device is shown in Fig. 2.
- TURN command: The user is requested to rotate around the current pose. The rotation angle is calculated by the IMU.
- MOVE command: The user is requested to move forward, with the device facing to the same direction. During the movement, received signal phase measurements are collected by the RFID reader, and used to calculate the displacement of the user.

Fig. 1. Photograph of a prototype of the proposed device. The device is held so that the antenna is pointing in front of the user, and performs a "scanning" movement, as explained in section II. The target estimation appears as a red dot on the device's display, where the distance and the direction to it are indicated.

Exploiting particle filters, consecutive executions of the above commands are used to improve the estimation of the distance and direction of the target RFID tag, as explained in section II-E.
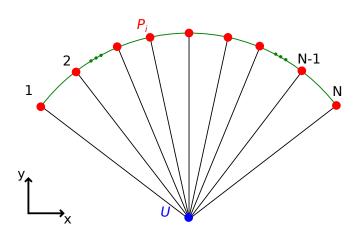
Fig. 2. A top view illustration of the positions of the device during a SCAN command. The blue circle is position **U** of the user. The red dots represent the positions $\mathbf{P}_i$ of the device. It is assumed that the positions of the device are on a circular trajectory: the distance between the device and the user is constant.

A. Measured Data

The proposed method leverages data measured by an RFID reader and a 9DoF IMU. The RFID reader measures the phase of the target-tag's backscattered signal which is wrapped in $[0, \pi)$. Thanks to the reader's read-rate, the wrapping points can be recognized and the phase measurement is unwrapped. Additionally, real measurements include noise, which is modeled as a normally distributed variable. So, the measured phase is:

$$\phi_{meas} = (\phi + \phi_{noise}) \ mod \ (\pi) \tag{1}$$

$$\phi = \phi_p + \phi_o \tag{2}$$

$$\phi_p = \frac{4\pi}{\lambda} d \tag{3}$$

$$\phi_{noise} \sim N(0, s_{phase}), \tag{4}$$

where ϕ is the phase of the received signal, ϕ_p is the phase accumulated due to the electromagnetic wave propagation, ϕ_o is a phase offset including phases of the cables and the related hardware, ϕ_{noise} is the phase measurement noise, λ is the wavelength of the electromagnetic field, and d is the distance from the antenna to the tag.

The 9DoF IMU measures the angle around the desired axis. In our case, it measures the angle of the device during SCAN and TURN commands. The value of the device's angle was calculated using the Madgwick orientation algorithm [23]. The measurements are in $[0, 2\pi)$, and, like the phase measurements, unwrapping is required. Additionally, they include noise originating from the IMU as well as the user. Let the angle measured by the IMU be:

$$\theta_{meas} = (\theta + \theta_{noise}) \ mod \ (2\pi) \tag{5}$$

$$\theta_{noise} \sim N(0, s_{angle}), \tag{6}$$

where θ is the real angle, and θ_{noise} is the measurement's noise. Experiments were conducted to evaluate the mean and standard deviation of the angular error of the IMU. It was found that the mean error was 0.2^o and the standard deviation $s_{angle} = 2^o$.

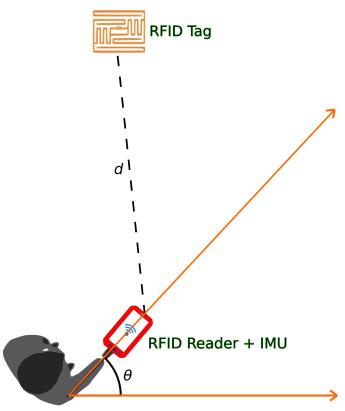An illustration of how the measured data are collected is shown in Fig. 3.

Fig. 3. Illustration of the data measured by the proposed handheld device: The RFID Reader measures the received signal phase value, which is a function of the distance d between the RFID Reader and the target RFID Tag. The IMU measures the angle of the device's position relative to an arbitrary direction.

B. Single Measurement Target Estimation

During the SCAN command it is assumed that the device is moved on a circular trajectory parallel to the ground, as shown in Fig. 2. The user is facing towards the y-axis of a local user-centered coordinate system. $\mathbf{U} = [0, 0]$ is the position of the user. Initially the device is also facing towards the y-axis. Let the position of the device at the beginning of the scanning be $\mathbf{P}_{start}$. On the local coordinate system:

$$\mathbf{P}_{start}(a) = [0, a] \tag{7}$$

where a is the radius of the circular trajectory. Since the device is operated by human users, a is **not** known, it depends on how the user moves the device. As it is shown in section II-E, the proposed method assumes and estimates the device rotation radius.

Let's assume that phase and rotation angle measurements are collected in N positions $\mathbf{P}_i$, $i = \{1, 2, \ldots, N\}$. The unwrapped phase and rotation angle measurements at position

$\mathbf{P}_i$ are ϕ_i and θ_i. Let the rotation angle measurement at the beginning of the scanning be θ_{start}. The relative rotation of position i to the beginning of the measurements is:

$$rot_i = \theta_i - \theta_{start} \qquad (8)$$

The position $\mathbf{P}_i$ is:

$$\mathbf{P}_i(a) = [-a\ sin\ (rot_i)\ , a\ cos\ (rot_i)] \qquad (9)$$

Assuming that a is known, the target tag position estimation $\mathbf{T}$ can be calculated by solving the following minimization problem:

$$\mathbf{T}(a) = \arg\min_{\hat{\mathbf{T}}} f_{cost}\left(\hat{\mathbf{T}}, a\right) \qquad (10)$$

$$f_{cost}\left(\hat{\mathbf{T}}, a\right) = \sum_{i=1}^{N} \sum_{j=i+1}^{N} \left(\Delta\phi_{i,j} - \Delta|\hat{\mathbf{T}}\mathbf{P}|_{i,j}(a)\right)^2 \qquad (11)$$

$$\Delta\phi_{i,j} = \phi_i - \phi_j \qquad (12)$$

$$\Delta|\hat{\mathbf{T}}\mathbf{P}|_{i,j}(a) = \frac{4\pi}{\lambda}\left(||\hat{\mathbf{T}} - \mathbf{P}_i(a)||_2 - ||\hat{\mathbf{T}} - \mathbf{P}_j(a)||_2\right) \qquad (13)$$

$||\hat{\mathbf{T}} - \mathbf{P}_i(a)||_2$ is the euclidean distance between points $\hat{\mathbf{T}}$ and $\mathbf{P}_i(a)$. Equation (11) is a metric of the similarity of the measured phase to the theoretical measurements if the target was at $\hat{\mathbf{T}}$. An illustration of the values involved in the minimization problem is shown in Fig. 4. The estimated distance D_{est} and angle A_{est} are calculated relative to the user position $\mathbf{U}$ and the positive y-axis direction:
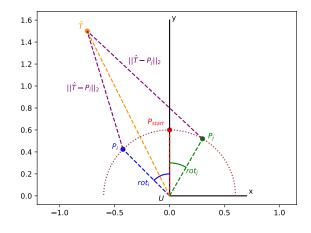

Fig. 4. An illustration of the values involved in the minimization problem of section II-B: $\mathbf{U}$ is the position of the user, and $\mathbf{P}_{start}$ is the initial position of the device. $\mathbf{P}_i, \mathbf{P}_j$ are two of the positions of the device during the scan movement. The corresponding rotation angles rot_i, rot_j are measured with respect to the initial position of the device. $\mathbf{P}_{start}$, $\mathbf{P}_i$, $\mathbf{P}_j$ are on the dotted brown circle of radius a. a is the assumed device rotation radius. $\hat{\mathbf{T}}$ is the assumed target position on which the cost function (11) is calculated. $||\hat{\mathbf{T}} - \mathbf{P}_i||_2$ and $||\hat{\mathbf{T}} - \mathbf{P}_j||_2$ are the distances used in (13). Axis dimensions are in meters (m).

$$D_{est} = ||\mathbf{U} - \mathbf{T}||_2 \qquad (14)$$

$$A_{est} = \angle\left(\bar{\mathbf{U}}\mathbf{T}\right) - \pi/2 \qquad (15)$$

$\angle\left(\bar{\mathbf{U}}\mathbf{T}\right)$ is the angle of $\bar{\mathbf{U}}\mathbf{T}$ vector.

C. Rotation Radius Assumption's Effect on Target Estimation

As mentioned in section II-B, the real rotation radius a is not known in our case and its value is assumed. Next, we examine how the target estimation is affected by the assumed rotation radius a_{smd}. Let the user's position be $\mathbf{U}$, and the real position of the target be $\mathbf{T}_{real}$. To evaluate the estimations, the relative to the user distance and angle of the estimated target $\mathbf{T}(a_{smd})$ are compared to the real values:

$$D_{err}\left(\mathbf{T}(a_{smd})\right) = D_{err}\left(a_{smd}\right) = $$
$$= |(||\mathbf{U} - \mathbf{T}_{real}||_2 - ||\mathbf{U} - \mathbf{T}||_2)| \qquad (16)$$

$$A_{err}\left(\mathbf{T}(a_{smd})\right) = A_{err}\left(a_{smd}\right) = $$
$$= |\angle\left(\bar{\mathbf{U}}\mathbf{T}_{real}\right) - \angle\left(\bar{\mathbf{U}}\mathbf{T}\right)| \qquad (17)$$

Measurements in ideal conditions are simulated: noiseless phase and rotation angle measurements are collected, the device is rotated $\pm45^o$, $a = 0.5m$. The target $\mathbf{T}_{real}$ is randomly generated in distinct distances $1m$ to $10m$ from the target, and distinct rotation angles a_{smd} in $[0.45m, 0.55m]$ are assumed. The target's position $\mathbf{T}$ is estimated by solving (10) using an unbounded minimization method. Thanks to phase unwrapping, the solution is calculated rapidly, since the cost function is convex. Therefore, during application of the method in the actual environment, we expect to have the estimated location of the tag in real-time, which represents an important constraint of our system. A_{err} and D_{err} are shown in Fig. 5 and Fig. 6, respectively. When the correct radius is considered, i.e. $a = 0.5m$, the location of the tag is estimated correctly; thus validating the proposed method.

Correct estimation of the direction of the target is not affected by the unknown radius of the human, as demonstrated in Fig. 5. A_{err} values are insignificant considering the user is human, whose angular perception is limited. This is due to the fact, that the direction of the target is identified at the recorded angle of the minimum of the measured unwrapped phase; this point is not affected by the radius a, but is expected to suffer from the Gaussian noise of the two involved measurements' devices, the reader and the IMU, which are not considered in these simulations.

However, Fig. 6 shows that the distance estimation is heavily dependent on the accurate assumption of the rotation radius. Additionally, as the distance of the target increases, so does the estimation distance error. Only when the real rotation radius is assumed the minimization problem converges to the target's position regardless of the distance, as indicated by the purple line of Fig. 6. It is also noted that the value of the cost function (11) in this case is in the order of 10^{-7}. On the other hand, for assumed rotation radius different than the real one, the cost function value is in the order of 10^{-2}.
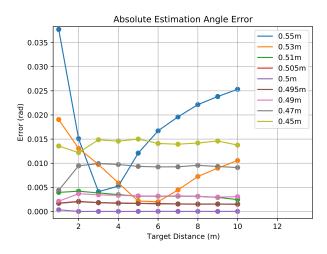
Fig. 5. A_{err} from (17) calculated by simulations for different assumed rotation radii a_{smd} in ideal conditions. The real distance between the target and the user is shown in x-axis. The real rotation radius is $a = 0.5m$. Different lines show the error for the corresponding a_{smd} in the y-axis.
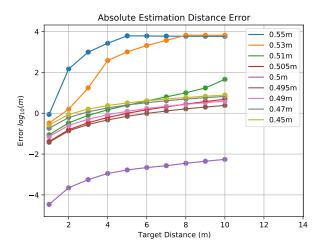

Fig. 6. D_{err} from (16) calculated by simulations for different assumed rotation radii a_{smd} in ideal conditions. The real distance between the target and the user is shown in x-axis. The real rotation radius is $a = 0.5m$. Different lines show the error for the corresponding a_{smd} in the y-axis (logarithmic scale).

As mentioned above, the results presented in Fig. 5 and Fig. 6 are calculated by solving (10) with an unbounded minimization method. Thus, target estimations at great distances from the user can be calculated. This however cannot be true in a real world scenario, since the RFID tags are readable within a limited range. So, we now examine the same problem, but limiting the solution search area in a 20m x 20m square in front of the user. The limits of the area match the maximum reading range of COTS passive RFID tags. Simulations similar to those of Fig. 6 are repeated, with the addition of phase measurement noise $\phi_{noise} \sim N(0, 0.1\ (rad))$, and rotation angle measurement noise $\theta_{noise} \sim N(0, 1^o)$. $s_{phase} = 0.1\ (rad)$ is the typical standard deviation of the received phase measurement noise of a COTS RFID reader, and $s_{angle} = 1^o$ was measured on the used IMU. D_{err} is

calculated once again, along with the corresponding value of the minimized cost function (11).

The results are shown in Fig. 7. Lower cost function values still correspond to lower error solutions. This means that we can use the cost function value as a criterion to evaluate target position estimations.

It is noted that the proposed method will be affected by more ambiguity factors than just the phase and angle measurement noise. RFID communication is affected by multipath. Rotation angle measurements require correct calibration. Finally, since the operator is human, the device's trajectory cannot be perfectly circular.

So, to improve the estimation of the target's position, we leverage multiple SCAN measurements, instead of just one, using a particle filter algorithm, as shown in section II-E.
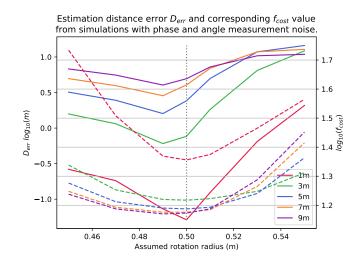

Fig. 7. D_{err} from (16) and f_{cost} from (11) calculated by simulations with phase and angle measurement noise for different assumed rotation radii a_{smd}, as explained in section II-C. Different colors represent different distances between the user and the target. The real rotation radius is $a = 0.5m$, marked with a gray dotted line. The assumed rotation radius a_{smd} is shown on the x-axis. Continuous lines correspond to D_{err} values on the left vertical axis, and dashed lines to f_{cost} values on the right. Both vertical axes are shown in logarithmic scale.

D. Antenna and Target Height Difference

In this section we examine how the target estimation is affected by the unknown height difference dh between the reader's antenna and the target. So far, it is assumed that the antenna and the target tag are on the same height. Simulations in ideal conditions are conducted, similarly to section II-C. The solution search area is a 20m x 20m square in front of the user. The height difference dh between the antenna and the target is unknown.

The results are shown in Fig. 8 and Fig. 9. Fig. 8 shows that the angle estimation error is very low regardless of the height difference dh. Its maximum value is $\sim 1.7^o$, which is satisfactory for human related applications. So, the device will always guide the user to the correct direction regardless of the height of the tag.

The distance estimation errors presented in Fig. 9 reveal that when the antenna is far from the target and a wrong rotation
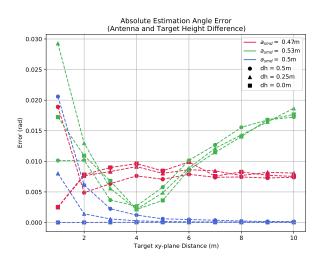
Fig. 8. A_err from (17) calculated by simulations for different assumed rotation radii a_{smd} and unknown height differences dh between the reader's antenna and the target tag, in ideal conditions. The real distance on the xy-plane between the target and the user is shown in the horizontal axis. The real rotation radius is $a = 0.5m$. Same color lines show the error for the corresponding a_{smd} for different values of dh, indicated by different plot markers.
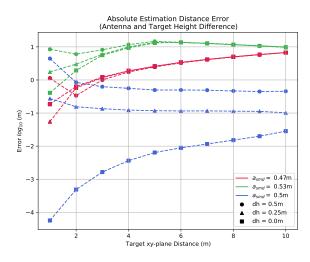

Fig. 9. D_{err} from (16) calculated by simulations for different assumed rotation radii a_{smd} and unknown height differences dh between the reader's antenna and the target tag, in ideal conditions. The real distance on the xy-plane between the target and the user is shown in the horizontal axis. The real rotation radius is $a = 0.5m$. Same color lines show the error (logarithmic scale) for the corresponding a_{smd} for different values of dh, indicated by different plot markers.

radius is assumed, the estimation is not affected. If the correct radius is assumed, the distance error is $\sim dh$. It is expected that, if the height difference is a small portion of the total distance from the antenna to the tag, the estimation results will not be affected.

The proposed method does not provide a way to indicate the direction of target in 3D. An extension of the method could leverage the orientation in 3D space provided by the IMU, to estimate the position of the target in three dimensions. In our case, however, the proposed device will be used in the

Archeological Museum of Thessaloniki, where the tags will be placed in the same height at which a typical user would hold the RFID reader.

E. Particle Filter Algorithm

In this section the implemented Particle Filter Algorithm is presented. The algorithm is used to leverage measurement from consecutive execution of the three commands described in section II: SCAN, TURN, and MOVE commands. A pseudo code implementation of the algorithm is shown in Algorithm 1.

Algorithm 1: Proposed Algorithm

create initial particles;
# begin iterative process ;
iterationFlag = True ;
while *iterationFlag* **do**
    execute SCAN command;
    assign weights to particles;
    estimate Target;

    if *Target distance < distance threshold* **then**
        # target was found ;
        iterationFlag = False;
    else
        execute TURN command;
        calculate rotation angle;
        update particles;

        execute MOVE command;
        calculate step for each particle;
        update particles;

        RESAMPLE particles;
    end
end

---

1) SCAN Command: Initially, M randomly generated particles are created. Particle p_m^l is the m-th of M particles during the l-th iteration. They represent a possible user pose relative to the target $\mathbf{T}_{ar} = [0, 0]$. p_m^l is defined by the following values:

- $\mathbf{K}_m^l = [x_m^l, y_m^l]$ is a complex number representing the user's coordinates on the xy-plane.
- $\bar{\mathbf{V}}_m^l$ is a complex number representing the direction on the xy-plain the user is facing to.
- a_m^l is the device rotation radius of the user.
- w_m^l is the weight assigned to the particle. All particle weights are initially equal to 1.

After the initialization, the iterative process begins. A SCAN command is executed. This results to measurement set $Meas^l$ consisting of phase and rotation angle measurements:

$$Meas^l = \left[\phi_n^l, rot_n^l\right], \ n = 1, \dots, N \qquad (18)$$

ϕ_n^l and rot_n^l are the N pairs of phase and rotation angle measurements indicated by n during the l-th iteration, as

described in section II-B. Using the rotation angle measurements, the positions $\mathbf{Q}_{m,n}^l$ of the device during the scan that correspond to each particle p_m^l can be calculated:

$$\mathbf{Q}_{m,n}^l = \left[x_m^l + a_m^l \, cos\left(\angle\left(\bar{\mathbf{V}}_m^l\right) + rot_n^l \right), \\ y_m^l + a_m^l \, sin\left(\angle\left(\bar{\mathbf{V}}_m^l\right) + rot_n^l \right) \right] \quad (19)$$

$\mathbf{Q}_{m,n}^l$ would be the positions of the device, if the user's position, facing direction, and rotation radius were those of particle p_m^l: $\mathbf{K}_m^l$, $\bar{\mathbf{V}}_m^l$, a_m^l. An illustration of $\mathbf{Q}_{m,n}^l$ points of different particles p_m^l is shown in Fig. 10.
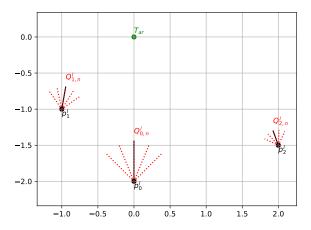

Fig. 10. $\mathbf{Q}_{m,n}^l$ points of different particles p_m^l, $m = 1, 2, 3$. The black line segments starting from the particle centers $\mathbf{K}_m^l$ indicate the direction of $\mathbf{V}_m^l$, and its length is equal to a_m^l. Their endpoints represent the assumed initial position of the device. The measured rotation angles rot_n^l, $n = 1, \ldots, 5$ are used to calculate points $\mathbf{Q}_{m,n}^l$ for each particle: the the device is rotate around the particle's center according to the measurements. $\mathbf{T}_{ar}$ is assumed position of the target. Axis dimensions are in meters (m).

A new normalized weight h_m^l for each particle p_m^l is calculated:

$$h_m^l = \frac{w_m^l / g_{cost}(m,l)}{\displaystyle\sum_{q=1}^{M} w_q^l / g_{cost}(q,l)} \quad (20)$$

$$g_{cost}(m,l) = \sum_{i=1}^{N} \sum_{j=i+1}^{N} \left(\Delta\phi_{i,j}^l - \Delta|\mathbf{T}_{ar}\mathbf{Q}_m|_{i,j}^l \right)^2 \quad (21)$$

$$\Delta\phi_{i,j}^l = \phi_i^l - \phi_j^l \quad (22)$$

$$\Delta|\mathbf{T}_{ar}\mathbf{Q}_m|_{i,j}^l = \frac{4\pi}{\lambda} \left(||\mathbf{T}_{ar} - \mathbf{Q}_{m,i}^l||_2 \right) \\ - \frac{4\pi}{\lambda} \left(||\mathbf{T}_{ar} - \mathbf{Q}_{m,j}^l||_2 \right) \quad (23)$$

w_m^l in (20) is the weight of the specific particle from the previous iteration $l - 1$, which ensures the memory of each particle is kept. w_m^l will be given explicitly after the "Resampling" process in (43). The theoretical phase difference is

calculated in (23), as in (13). Equation (22) is the measured phase difference. g_{cost} of (21) is a cost function similar to (11). It evaluates the similarity of theoretical phase difference and measured phase difference assuming that the user's position, facing direction, and rotation radius were those of particle p_m^l: $\mathbf{K}_m^l$, $\bar{\mathbf{V}}_m^l$, a_m^l. Finally, in (20) the weight value of the particle is divided by the value of the cost function $g_{cost}(m,l)$, and is normalized so that the sum of the normalized weight h_m^l is 1:

$$\sum_{m=1}^{M} h_m^l = 1 \quad (24)$$

In section II-C, we concluded that low cost function values correspond to lower error estimations. So, low $g_{cost}(m,l)$ values correspond to higher h_m^l values, if the effect of the previous weight value w_m^l is ignored.

Having assigned normalized weights to all particles, the one with the highest normalized weight is is used to estimate the targets position:

$$b^l = \arg\max_m \left(h_m^l \right) \quad (25)$$

$$D_{est}^l = ||\mathbf{K}_{b^l}^l - \mathbf{T}_{ar}||_2 \quad (26)$$

$$A_{est}^l = \angle\left(\mathbf{K}_{b^l}^l \bar{\mathbf{T}}_{ar} \right) - \angle\left(\bar{\mathbf{V}}_{b^l}^l \right) \quad (27)$$

Equation (26) is the distance of the b^l-th particle's center to the assumed target position, and (27) is the angle difference between the vector from the particle's center to the assumed target (which is the direction of the target, if the user was standing on the particle's position) and the particle's direction $\bar{\mathbf{V}}_{b^l}^l$.

If D_{est}^l is lower than a threshold D_{thresh}, the iterative process is finished.

2) TURN Command: The user is asked to rotate around the current position towards the estimated target. As the user rotates, new rotation angle measurements are collected. By comparing the unwrapped initial and final angle measurements, the turn angle $turn^l$ can be calculated. Every particle's $\bar{\mathbf{V}}_m^l$ value is updated according to $turn^l$ and a random variable θ_{jit}. The updated value is $\bar{\mathbf{Vu}}_m^l$:

$$\bar{\mathbf{Vu}}_m^l : \begin{cases} \angle\left(\bar{\mathbf{Vu}}_m^l \right) = \angle\left(\bar{\mathbf{V}}_m^l \right) + turn^l + \theta_{jit} \\ |\bar{\mathbf{Vu}}_m^l| = 1 \end{cases} \quad (28)$$

$$\theta_{jit} \sim N(0, s_\theta^{jit}) \quad (29)$$

θ_{jit} is used as an accommodation to the noisy angle measurements.

3) MOVE Command: The user is asked to move straight ahead, towards the facing direction. The unwrapped phase difference $\Delta\phi_{step}^l$ between the final and initial position is measured and used to calculate the move distance of each particle. Let $\mathbf{A}_m^l$ be the initial phase measurement point and $\mathbf{B}_m^l$ the final one.

The RFID tag is at $\mathbf{C}_m^l$ as shown in Fig. 11. Our goal is to calculate the distance $||\mathbf{A}_m^l - \mathbf{B}_m^l||_2$. $\Delta\phi_{step}^l$ is:

$$\Delta\phi_{step}^l = \frac{4\pi}{\lambda}\left(||\mathbf{C}_m^l - \mathbf{B}_m^l||_2 - ||\mathbf{C}_m^l - \mathbf{A}_m^l||_2\right) \quad (30)$$

Using the cosine law for triangle $(\mathbf{ABC})_m^l$ and (30):

$$\left(||\mathbf{A}_m^l - \mathbf{B}_m^l||_2\right)^2 + R_{1m}^l||\mathbf{A}_m^l - \mathbf{B}_m^l||_2 + R_{2m}^l = 0 \quad (31)$$

R_{1m}^l and R_{2m}^l are:

$$R_{1m}^l = -2||\mathbf{C}_m^l - \mathbf{A}_m^l||_2 \, cos\left(\left(\mathbf{C\hat{A}B}\right)_m^l\right) \quad (32)$$

$$R_{2m}^l = 2||\mathbf{C}_m^l - \mathbf{A}_m^l||_2 \frac{\Delta\phi_{step}^l \, \lambda}{4\pi} - \left(\frac{\Delta\phi_{step}^l \, \lambda}{4\pi}\right)^2 \quad (33)$$

Solving (31) for each particle p_m^l results to the corresponding move distance $step_m^l = ||\mathbf{A}_m^l - \mathbf{B}_m^l||_2$. For p_m^l the corresponding values of $\mathbf{A}_m^l$, $\mathbf{C}_m^l$, and $\left(\mathbf{C\hat{A}B}\right)_m^l$ are:

$$\mathbf{A}_m^l = \mathbf{K}_m^l + a_m^l \, \bar{\mathbf{V}}\mathbf{u}_m^l$$
$$\mathbf{C}_m^l = \mathbf{T}_{ar} \quad (34)$$
$$\left(\mathbf{C\hat{A}B}\right)_m^l = \angle\left(\bar{\mathbf{V}}\mathbf{u}_m^l\right) - \angle\left(\mathbf{A}_m^l\mathbf{C}_m^l\right)$$

We update the particle center values accordingly. The updated particle centers are $\mathbf{Ku}_m^l$:

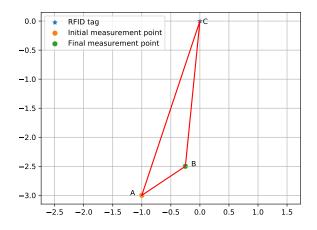$$\mathbf{Ku}_m^l = \mathbf{K}_m^l + step_m^l \, \bar{\mathbf{V}}\mathbf{u}_m^l \quad (35)$$

Fig. 11. Top view illustration of the user's movement. The user moves in a straight line from the initial position $\mathbf{A}$ towards the facing direction, and reaches the final position $\mathbf{B}$. As the user moves from $\mathbf{A}$ to $\mathbf{B}$, phase measurements from the RFID tag at point $\mathbf{C}$ are collected. The move distance $||\mathbf{A} - \mathbf{B}||_2$ can be calculated if the target's position and direction is known. Axis dimensions are in meters (m).

4) Resampling: The aim of resampling during the ongoing l^{th} iteration is to replace the current particles with new ones, generating more particles near poses (particles) with greater weight [24]. We create a discrete cumulative distribution function $C_{df}(m,l)$ that is used to decide which particles will be resampled:

$$C_{df}(m,l) = \sum_{i=1}^{m} h_i^l, \ m = 1, \ldots, M \quad (36)$$

Apparently, $C_{df}(M,l) = 1$. M numbers r_m^l are uniformly generated in $[0,1]$. r_m^l are matched to $C_{df}(m,l)$ to create the particle for the next iteration as follows:

$$t_m^l = \arg\min_{w}\left(w : C_{df}(w,l) \geq r_m^l\right) \quad (37)$$

Each t_m^l indicates which of the M current particles will "participate" in the next iteration $l+1$ of the algorithm. If a particle's normalized weight h_m^l is high, multiple t_m^l can be matched to it, which mean that multiple copies of it will participate in the next iteration. An example of how (37) works is shown in Fig. 12.
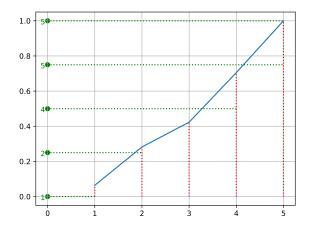

Fig. 12. An example of how t_m^l of (37) are calculated for $M = 5$. The blue line is $C_{df}(m,l)$. The green dots on the y-axis represent the r_m^l values, uniformly distributed in $[0,1]$. The corresponding t_m^l of each r_m^l is noted with green next to its dot. Multiple t_m^l can have the same value, as shown in the presented in which two of them have the value 5.

Now, the values of the particles p_m^{l+1} for the next iteration can be calculated as follows:

$$\mathbf{K}_m^{l+1} = \mathbf{Ku}_{t_m^l}^l + [x_{jit}, y_{jit}] \quad (38)$$

$$x_{jit} \sim N\left(0, s_{xy}^{jit}\right), \ y_{jit} \sim N\left(0, s_{xy}^{jit}\right) \quad (39)$$

$$\bar{\mathbf{V}}_m^{l+1} = \bar{\mathbf{V}}\mathbf{u}_{t_m^l}^l \quad (40)$$

$$a_m^{l+1} = a_{t_m^l}^l + a_{jit} \quad (41)$$

$$a_{jit} \sim N\left(0, s_a^{jit}\right) \quad (42)$$

$$w_m^{l+1} = h_{t_m^l}^l \qquad (43)$$

The random variables of (39) and (42) are used to differentiate the new particles from one another. This practice is called *jittering*. As stated before, multiple copies of the same particle can be chosen for the next iteration. So, by adding the jittering variables, greater particle diversity is achieved. An illustration of the result of jittering is shown in Fig. 13.
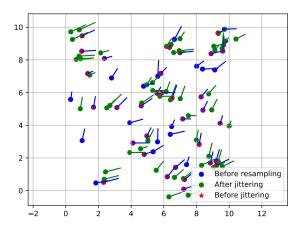
Then, the iterative process is repeated.

Fig. 13. Illustration of the resampling process. The dots represent the position $\mathbf{K}_m^l$ of the particles, the lines the direction $\bar{\mathbf{V}}_m^l$, and the length of each line the corresponding rotation radius a_m^l. The old blue particles are being resampled. The particles resampled at least once are marked red. The green ones are the new particle set, after jittering. Axis dimensions are in meters (m).

III. EXPERIMENTAL RESULTS

In this section experimental results are presented. Two experiment sets are described:

- $ExpSet1$: In the first set, the human user is trying to locate the target in a low multipath environment. The initial distance to the target tag is about $3m$. The user makes steps of about $41cm$ towards a predetermined direction, performing a SCAN command after each step, and not rotating according to the device's suggestions/indications. By examining $ExpSet1$ we aim to evaluate the accuracy of the target direction estimation, even when the user is not facing the target.
- $ExpSet2$: The experiments of the second test are conducted in high multipath environment, a computer lab of the School of Electrical and Computer Engineering of Aristotle University of Thessaloniki. The initial distance to the target is $6m$. The user makes steps of about $1m$ or $1.5m$, performing a SCAN command after each step, moving towards the target. By examining $ExpSet2$ we aim to evaluate the performance of the target distance estimation in a multipath rich environment.

A. $ExpSet1$ Results

Here the setup of experiment set $ExpSet1$ is described, and the proposed method's results are presented. $ExpSet1$ consists

of three experiments: $1.A$, $1.B$, $1.C$. These experiments are carried out in a low multipath environment. An illustration of the user's movement during each experiment is shown in Fig. 14. The user moves in a straight line towards the positive y-axis direction. The distance of two consecutive positions is $41cm$. In every experiment, the initial y-axis distance between the user and the target is the same, but the x-axis distance is different. This results to different initial angle between the user and the target in each experiment: in $1.A$ that angle is $\sim 15.9^o$, in $1.B \sim 8.1^o$, in $1.C$ 0°.
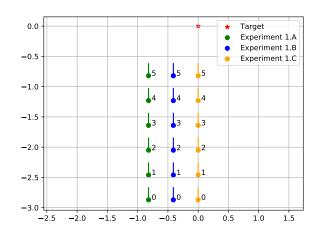

Fig. 14. Top view illustration of $ExpSet1$ user poses. The red marker is the position of the target. Each of the remaining colors represent one experiment: the dots show the position of the user, and the line segments the direction the user is facing to in the corresponding position. The numbers next to each pose indicate the chronological order of the poses in the corresponding experiment. Axis dimensions are in meters (m).

The aim of $ExpSet1$ is to evaluate the accuracy of the target direction estimation, even when the user is not facing the target. The distance and angle estimation expected absolute errors are shown in Table I. The following parameter values were used: $M = 1000$, $N = 20$, $s_{xy}^{jit} = 0.05m$, $s_{\theta}^{jit} = 3^o$, $s_a^{jit} = 0.05m$.

In experiments $1.A$ and $1.B$ the angle estimation error is small for all the algorithm steps, its max value being $\sim 9^o$. In $1.C$ the angle estimation has higher error values, averaging around $\sim 15^o$. The results of $1.A$ and $1.B$ are satisfactory for human related applications, and those of $1.C$ are deemed acceptable. As for the distance estimation, only experiment $1.C$ grants satisfactory results. The distance estimations appear to follow a sequence resembling that of the corresponding ground truth values. In experiments $1.A$ and $1.B$ as the user moves forward, the angle of the devices facing direction and the target increases, meaning that during the scanning the target is visible by the antenna in a smaller angular range. Thus, the collected data are fewer which leads to poor distance estimation performance.

Additionally, the increasing angle in experiments $1.A$ and $1.B$ leads to the trajectory of the antenna during the scanning motion to resemble a linear trajectory on a line parallel to the direction the target. This, however, maximizes the POA measurement ambiguity. Successful Synthetic Aperture Radar

(SAR) methods rely on measurements collected on the complete opposite, that is trajectories perpendicular to the direction of the target. In experiment $1.C$ on the other hand, the user moves towards the target, and more favorable measurement conditions are met.

TABLE I
$ExpSet1$ DISTANCE (m) AND ANGLE (deg) ESTIMATIONS, AND CORRESPONDING ERRORS, AS EXPLAINED IN SECTION III-A.

Experiment 1.A

	Distance (m)			Angle (deg)		
Index	Est.	G.T.	Error	Est.	G.T.	Error
0	1.31	3.18	-1.87	-18.1	-14.9	-3.2
1	2.20	2.79	-0.59	-22.4	-17.1	-5.3
2	4.13	2.40	1.73	-20.8	-20.0	-0.8
3	4.30	2.02	2.28	-19.0	-24.0	5.0
4	4.23	1.65	2.58	-20.9	-29.7	8.8
5	3.09	1.31	1.78	-34.0	-38.7	4.7

Experiment 1.B

	Distance (m)			Angle (deg)		
Index	Est.	G.T.	Error	Est.	G.T.	Error
0	7.96	3.10	4.86	-3.8	-7.6	3.8
1	2.89	2.70	0.19	-7.0	-8.7	1.7
2	2.36	2.29	0.07	-15.7	-10.3	-5.4
3	2.83	1.89	0.94	-13.2	-12.5	-0.7
4	2.90	1.49	1.41	-19.0	-15.9	-3.1
5	2.73	1.10	1.63	-19.3	-21.8	2.5

Experiment 1.C

	Distance (m)			Angle (deg)		
Index	Est.	G.T.	Error	Est.	G.T.	Error
0	2.55	3.07	-0.52	-11.7	0	-11.7
1	0.89	2.66	-1.77	16.2	0	16.2
2	2.46	2.26	0.20	-6.7	0	-6.7
3	0.78	1.84	-1.06	-17.2	0	-17.2
4	1.20	1.43	-0.23	-12.4	0	-12.4
5	1.24	1.03	0.21	-20.6	0	-20.6

*Est. := Estimation, G.T. := Ground Truth,
Error := Est. - G.T.
**Algorithm parameters: $M = 1000$, $N = 20$,
$s_{xy}^{jit} = 0.05m$, $s_{\theta}^{jit} = 3^o$, $s_{a}^{jit} = 0.05m$.

B. $ExpSet2$ Results

Here the setup of experiment set $ExpSet2$ is described, and the proposed method's results are presented. $ExpSet2$ consists of three experiments: $2.A$, $2.B$, $2.C$. These experiments are conducted in a multipath rich environment, a computer lab of the School of Electrical and Computer Engineering of Aristotle University of Thessaloniki. An illustration of the user's movement during each experiment is shown in Fig. 15. Based on the observations made in section III-A, the user is moving in a straight line towards the target. Experiments $2.A$ and $2.B$ are identical. The initial distance from the target is 6m, and the user moves towards it 1m at a time. In experiment $2.C$ the initial distance is 6m as well, but the user takes greater steps, three of 1.5m and one of 1m. It is noted that in each experiment, the user was not initially facing the target. To find the direction of the target, a wide-angle scanning motion is initially performed, and the user is guided towards the target.

The aim of $ExpSet2$ is to evaluate the performance of the target distance estimation in a multipath rich environment.
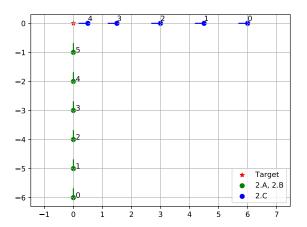

Fig. 15. Top view illustration of $ExpSet2$ user poses. The red marker is the position of the target. Each of the remaining colors represent one experiment: the dots show the position of the user, and the line segments the direction the user is facing to in the corresponding position. The numbers next to each pose indicate the chronological order of the poses in the corresponding experiment. Experiments 2.A and 2.B are identical. Axis dimensions are in meters (m).

The distance and angle estimation expected absolute errors are shown in Table II. The following parameter values were used: $M = 1000$, $N = 20$, $s_{xy}^{jit} = 0.05m$, $s_{\theta}^{jit} = 3^o$, $s_{a}^{jit} = 0.05m$.

In all three experiments the angle estimation error is always less than 10°, except for one out of the seventeen estimations. In all cases the user moves towards the target, similarly to experiment $1.C$. Comparing the results of $1.C$, presented in section III-A, to the results of $ExpSet2$, the angle estimation errors of the latter are significantly lower. This indicates that the errors of $1.C$ can be attributed to imperfect operation of the device.

As for the distance estimation, in all three experiments the results are satisfactory. We can see in Table II that after the first two or three algorithm's iterations, the estimation resembles the actual distance between the user and the target. In all cases, in the final iteration of the algorithm the error is less than $0.5m$.

C. Guiding Capabilities

In this section we examine the proposed method's capability to guide the user towards the target RFID tag. As the user executes the device's commands, after each SCAN command, the user is instructed to rotate towards the estimated target position.

First, we have to define what is considered successful guiding. Let the actual angle between the user's facing direction and the target at the l-th iteration be A_{actual}^l. The corresponding estimated angle is A_{est}^l. The user's rotation is $turn^l$ as in section II-E2.

Ideally, at the first iteration $l = 1$ the angle estimation is identical to the real angle: $A_{actual}^1 = A_{est}^1$. The user rotates accordingly: $turn^1 = A_{actual}^1$. So, in the following iterations, the actual and estimated target angle will be 0°, and the user will move forward towards the target:

TABLE II
$ExpSet2$ DISTANCE (m) AND ANGLE (deg) ESTIMATIONS, AND
CORRESPONDING ERRORS, AS EXPLAINED IN SECTION III-B.

Experiment 2.A

Index	Distance (m)			Angle (deg)		
	Est.	G.T.	Error	Est.	G.T.	Error
0	1.73	6.00	-4.27	4.3	0	4.3
1	4.09	5.00	-0.91	8.0	0	8.0
2	4.50	4.00	0.5	9.8	0	9.8
3	3.43	3.00	0.43	3.8	0	3.8
4	2.78	2.00	0.78	3.1	0	3.1
5	1.34	1.00	0.34	0.6	0	0.6

Experiment 2.B

Index	Distance (m)			Angle (deg)		
	Est.	G.T.	Error	Est.	G.T.	Error
0	1.73	6.00	-4.27	4.3	0	4.3
1	5.07	5.00	0.07	1.3	0	1.3
2	4.28	4.00	0.28	5.8	0	5.8
3	2.97	3.00	-0.03	-3.9	0	-3.9
4	2.45	2.00	0.45	-2.7	0	-2.7
5	1.40	1.00	0.4	-4.7	0	-4.7

Experiment 2.C

Index	Distance (m)			Angle (deg)		
	Est.	G.T.	Error	Est.	G.T.	Error
0	1.82	6.00	-4.18	7.2	0	7.2
1	2.28	4.50	-2.22	-4.2	0	-4.2
2	3.15	3.00	0.15	-17.1	0	-17.1
3	1.21	1.50	-0.29	-2.3	0	-2.3
4	0.97	0.50	0.47	-5.7	0	-5.7

*Est. := Estimation, G.T. := Ground Truth,
  Error := Est. - G.T.
**Algorithm parameters: $M = 1000$, $N = 20$,
  $s_{xy}^{jit} = 0.05m$, $s_{\theta}^{jit} = 3^o$, $s_a^{jit} = 0.05m$.

$$A_{actual}^l = A_{est}^l = turn^l = 0, \ l > 1 \quad (44)$$

In a more realistic approach, it would be assumed that the estimated angle includes an error A_{error}^l:

$$A_{est}^0 = A_{actual}^0 + A_{error}^l \quad (45)$$

We assume that the user rotates exactly as instructed, so $turn^0 = A_{est}^0$. The actual angle in the next iteration will be:

$$A_{actual}^1 = A_{actual}^0 - turn^0$$
$$A_{actual}^1 = A_{actual}^0 - A_{actual}^0 - A_{error}^0 \quad (46)$$
$$|A_{actual}^1| = |A_{error}^0|$$

Similarly:

$$|A_{actual}^{l+1}| = |A_{error}^l| \quad (47)$$

It is desired that at one point, after some iterations, the user will be facing the target, or $A_{actual}^l = 0$. A sufficient condition to achieve this is that the error of the estimated angle is lower than the actual angle:

$$|A_{error}^l| < |A_{actual}^l| \quad (48)$$

From (47), (48):

$$|A_{error}^l| < |A_{actual}^l| = |A_{error}^{l-1}|$$
$$|A_{error}^l| < |A_{error}^{l-1}| \quad (49)$$
$$|A_{error}^l| = \epsilon_l |A_{error}^{l-1}|, \epsilon_l \in [0, 1)$$

From (47), (49):

$$|A_{actual}^{l+1}| = \epsilon_l \ \epsilon_{l-1} \ \ldots \ \epsilon_1 |A_{error}^0|$$
$$|A_{actual}^{l+1}| \to 0 \quad (50)$$

Equation (50) shows that, if (48) is satisfied, A_{actual}^l and A_{error}^l are expected to decrease as more iterations are completed. Similarly, we can show that if (48) is not satisfied, A_{actual}^l and A_{error}^l will increase.

To examine if (48) is satisfied in our case, data from $ExpSet1$ and $ExpSet2$ are used. We calculate the real angle between the user's facing direction and the target, and compare it to the absolute angle estimation error presented in Tables I and II. The results are shown in Fig. 16. The experimental data are used to create a line showing the expected estimation error A_{error}^l as a function of the real angle A_{actual}^l. According to the analysis of this section, we can see that the user will be guided towards the target with an absolute angular error of $\sim 6^o$. Such an error is acceptable for human related applications.
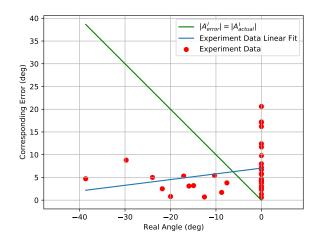

Fig. 16. Real angle between the user's facing direction and the target (x-axis), and the corresponding absolute estimation error (y-axis). On the green line the error is equal to the real angle: $|A_{error}^l| = |A_{actual}^l|$. The red dots are the experimental data, to which the blue line is linearly fitted. As long as the blue line is below the green one, the real angle and the corresponding error are expected to decrease as more algorithm iterations are completed.

D. Distance Estimation Errors

In this section the distance estimations of experiments are cumulatively presented. The examined experiments are $1.C$, $2.A$, $2.B$ and $2.C$, as explained in sections III-A and III-B. These are the experiments in which the user was moving towards the target, as it is intended according to the proposed method. $1.A$ and $1.B$ are not included since in these experiments the user did not attempt to go towards the target, which leads to inadequate measurement data as explained in section III-A.

In Fig. 17 the estimated absolute distance error as a function of the corresponding actual distance is presented. As the distance between the user and the target decreases, so does the distance estimation error. When the user has reached a distance of about $1m$ from the target, the distance estimation accuracy is about $40cm$. In Fig. 18 the distance estimation absolute normalized error, that is the distance estimation absolute error divided by the corresponding actual target distance, as a function of the corresponding iteration number is presented. It is shown that the more iterations are completed, the less significant the estimation error becomes.

E. Real Time Application

Here we examine the real time application capabilities of the proposed method. We record the computational time required on the handheld device to run the proposed method. Table III shows the computational time required by the device to run one algorithm iteration for different M, N parameter values. It is reminded that an iteration includes the SCAN, TURN, MOVE commands, and the resampling process. The resulted computational times reveal that the proposed method can be used in real time applications. Additionally, it is noted that even in the $M = 500$, $N = 10$ scenario, the distance estimation error in the last step remains low, at $61cm$.

TABLE III
EXPERIMENT 2.C REQUIRED COMPUTATIONAL TIME (C.T.) PER
ALGORITHM ITERATION FOR DIFFERENT M AND N PARAMETER VALUES.

M	N	C.T. (s)
1000	20	8.5
500	20	4.5
500	10	2.4

F. Real World Scenario Application Testing

In this section, results from testing the proposed method and prototype device in realistic scenarios are presented. Multiple testers were asked to use the device to help them locate a desired RFID tagged item. They were prompted by the device to execute the different motions and follow the displayed instructions.

After each SCAN command, the estimation of the target's distance and angle relative to the user's pose were shown on the device's display by means of displaying an arrow on the screen along with an estimated distance. The users were assisted by the device to follow the instruction by displaying a second arrow on the screen of their current pose. When both arrows were aligned, the user moves towards the proper direction. Their trajectories were monitored by a computer vision based measuring system, to get the ground truth position of the users.

The results are shown in Fig. 19. In all cases, the user was guided to the target. The distance errors were always positive, thus informing the user of greater distances than the actual. In all cases, the error was small when the user approached the target at an actual distance $\leq 1.7m$.

As the users approach the target, the distance estimated by the device helps them locate the target.
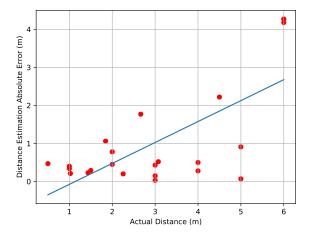

Fig. 17. Experiment target distance estimation absolute error (m) (y-axis), and corresponding actual distance (x-axis). The red dots are the experiment results, and the blue line linearly fitted to them. As the user moves towards the target, the error decreases.
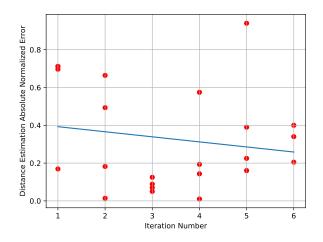

Fig. 18. Experiment target distance estimation absolute normalized error (y-axis) (that is the distance estimation absolute error divided by the corresponding actual target distance), and corresponding actual distance (x-axis). The red dots are the experiment results, and the blue line linearly fitted to them. As more algorithm iterations are completed, the target estimation improves.

IV. CONCLUSIONS AND FUTURE WORK

In this paper, we have presented a novel method for RFID tag localization using a handheld RFID reader and an IMU. We also designed and constructed a prototype of the proposed device. The user is instructed by the device to perform one of three actions: "SCAN", "TURN", and "MOVE". During these actions POA and rotation angle measurements are collected, and a PF algorithm leverages the data accordingly. Estimations of the direction and distance of the target are provided at the
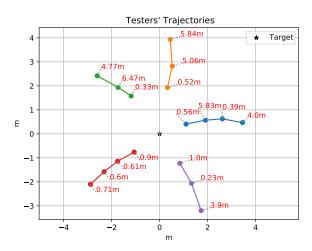
Fig. 19. Illustration of trajectories followed by users of the prototype of the proposed device. Each color represents a different user trajectory. The markers represent the positions where the corresponding user executed a SCAN command. Following the SCAN command, estimated distance and angle to the target were displayed to the users. They were instructed to follow the direction the device estimates. Each red number connected with a dotted line to a marker represents the distance estimation error at the corresponding position. As they were guided towards the target, the displayed estimated distance helped them locate the target.

end of each iteration. As more measurements are fused, the estimation is improved.

Experimental results showed high angle estimation accuracy with a mean error of $\sim 6^o$. When the user moved towards the target, according to the device's guidance, the distance estimation error was below $0.5m$ after few iterations. Additionally, the required computational time is deemed as suitable for real time applications, considering that the handheld device is operated by a human.

Future work will be focused on miniaturizing the device and improving its ease of use, providing a fluid user friendly experience. The first step to that direction is to automatically detect which of the commands was executed, without requiring user input: RFID Reader and IMU measurements will be used to detect which motion was performed. The natural flow of the user's motions will be tracked: we intend to allow the user to move freely, and not be limited by the current solutions three commands. The operation of the device's components can also be revamped to recognize and compensate for human operation related mistakes, and refine the data collection process.

As for the PF algorithm, our goal is to further reduce the required computational time, and integrate a way to evaluate the collected data in order to prevent ambiguous measurements from negatively affecting the algorithm's estimations.

REFERENCES

[1] S. Siachalou, A. Bletsas, J. Sahalos and A. G. Dimitriou, "RSSI-based maximum likelihood localization of passive RFID tags using a mobile cart," 2016 IEEE Wireless Power Transfer Conference (WPTC), 2016, pp. 1-4, doi: 10.1109/WPT.2016.7498847.
[2] D. Joho, C. Plagemann and W. Burgard, "Modeling RFID signal strength and tag detection for localization and mapping," 2009 IEEE International Conference on Robotics and Automation, 2009, pp. 3160-3165, doi: 10.1109/ROBOT.2009.5152372.
[3] J. Zhang, Y. Lyu, J. Patton, S. C. G. Periaswamy and T. Roppel, "BFVP: A Probabilistic UHF RFID Tag Localization Algorithm Using Bayesian Filter and a Variable Power RFID Model," in IEEE Transactions on Industrial Electronics, vol. 65, no. 10, pp. 8250-8259, Oct. 2018, doi: 10.1109/TIE.2018.2803720.
[4] A. Motroni, P. Nepa, P. Tripicchio and M. Unetti, "A Multi-Antenna SAR-based method for UHF RFID Tag Localization via UGV," 2018 IEEE International Conference on RFID Technology & Application (RFID-TA), 2018, pp. 1-6, doi: 10.1109/RFID-TA.2018.8552780.
[5] A. Tzitzis et al., "Localization of RFID Tags by a Moving Robot, via Phase Unwrapping and Non-Linear Optimization," in IEEE Journal of Radio Frequency Identification, vol. 3, no. 4, pp. 216-226, Dec. 2019, doi: 10.1109/JRFID.2019.2936969.
[6] A. Tzitzis, A. Raptopoulos Chatzistefanou, T. V. Yioultsis and A. G. Dimitriou, "A Real-Time Multi-Antenna SAR-Based Method for 3D Localization of RFID Tags by a Moving Robot," in IEEE Journal of Radio Frequency Identification, vol. 5, no. 2, pp. 207-221, June 2021, doi: 10.1109/JRFID.2021.3070409.
[7] A. Tzitzis, A. Malama, V. Drakaki, A. Bletsas, T. Yioultsis and A. G. Dimitriou, "Real-Time, Robot-Based, 3D Localization of RFID Tags, by Transforming Phase Measurements to a Linear Optimization Problem," in IEEE Journal of Radio Frequency Identification, doi: 10.1109/JRFID.2021.3103393.
[8] A. Motroni et al., "SAR-Based Indoor Localization of UHF-RFID Tags via Mobile Robot," 2018 International Conference on Indoor Positioning and Indoor Navigation (IPIN), 2018, pp. 1-8, doi: 10.1109/IPIN.2018.8533847.
[9] Longfei Shangguan and Kyle Jamieson. 2016. The Design and Implementation of a Mobile RFID Tag Sorting Robot. In Proceedings of the 14th Annual International Conference on Mobile Systems, Applications, and Services (MobiSys '16). Association for Computing Machinery, New York, NY, USA, 31–42. DOI:https://doi.org/10.1145/2906388.2906417
[10] E. DiGiampaolo and F. Martinelli, "Range and Bearing Estimation of an UHF-RFID Tag Using the Phase of the Backscattered Signal," in IEEE Journal of Radio Frequency Identification, vol. 4, no. 4, pp. 332-342, Dec. 2020, doi: 10.1109/JRFID.2020.3016168.
[11] K. Singh et al., "Localization of Life Safety Vests in an Aircraft Using Backscattering RFID Communication," in IEEE Journal of Radio Frequency Identification, vol. 4, no. 3, pp. 234-245, Sept. 2020, doi: 10.1109/JRFID.2020.3005248.
[12] M. Gareis, P. Fenske, C. Carlowitz and M. Vossiek, "Particle Filter-Based SAR Approach and Trajectory Optimization for Real-Time 3D UHF-RFID Tag Localization," 2020 IEEE International Conference on RFID (RFID), 2020, pp. 1-8, doi: 10.1109/RFID49298.2020.9244917.
[13] E. Giannelos, E. Andrianakis, K. Skyvalakis, A. G. Dimitriou and A. Bletsas, "Robust RFID Localization in Multipath With Phase-Based Particle Filtering and a Mobile Robot," in IEEE Journal of Radio Frequency Identification, vol. 5, no. 3, pp. 302-310, Sept. 2021, doi: 10.1109/JRFID.2021.3086759.
[14] F. Bernardini et al., "Particle Swarm Optimization in SAR-Based Method Enabling Real-Time 3D Positioning of UHF-RFID Tags," in IEEE Journal of Radio Frequency Identification, vol. 4, no. 4, pp. 300-313, Dec. 2020, doi: 10.1109/JRFID.2020.3005351.
[15] C. Li et al., "ReLoc: Hybrid RSSI- and Phase-Based Relative UHF-RFID Tag Localization With COTS Devices," in IEEE Transactions on Instrumentation and Measurement, vol. 69, no. 10, pp. 8613-8627, Oct. 2020, doi: 10.1109/TIM.2020.2991564.
[16] C. Li et al., "ReLoc 2.0: UHF-RFID Relative Localization for Drone-Based Inventory Management," in IEEE Transactions on Instrumentation and Measurement, vol. 70, pp. 1-13, 2021, Art no. 8003313, doi: 10.1109/TIM.2021.3069377.
[17] R. Mautz, "Indoor positioning technologies," Doctoral dissertation, Dept. Civil, Environ. Geomatic Eng., Inst. Geodesy Photogramm., ETH Zurich, Zurich, Switzerland, 2012
[18] P. Levchev, M. N. Krishnan, C. Yu, J. Menke and A. Zakhor, "Simultaneous fingerprinting and mapping for multimodal image and WiFi indoor positioning," 2014 International Conference on Indoor Positioning and Indoor Navigation (IPIN), 2014, pp. 442-450, doi: 10.1109/IPIN.2014.7275515.
[19] Gerstweiler G, Vonach E, Kaufmann H. HyMoTrack: A Mobile AR Navigation System for Complex Indoor Environments. Sensors (Basel). 2015 Dec 24;16(1):17. doi: 10.3390/s16010017. PMID: 26712755; PMCID: PMC4732050.
[20] U. Rehman and S. Cao, "Augmented-Reality-Based Indoor Navigation: A Comparative Analysis of Handheld Devices Versus Google Glass," in IEEE Transactions on Human-Machine Systems, vol. 47, no. 1, pp. 140-151, Feb. 2017, doi: 10.1109/THMS.2016.2620106.

[21] Mulloni, Alessandro & Seichter, Hartmut & Schmalstieg, Dieter. (2011). Handheld augmented reality indoor navigation with activity-based instructions. Mobile HCI 2011 - 13th International Conference on Human-Computer Interaction with Mobile Devices and Services. 211-220. 10.1145/2037373.2037406.

[22] A. Raptopoulos, T. Yioultsis and A. G. Dimitriou, "Particle Filter Object Tracking by a Handheld UHF RFID Reader," 2019 IEEE International Conference on RFID Technology and Applications (RFID-TA), 2019, pp. 342-347, doi: 10.1109/RFID-TA.2019.8892060.

[23] Madgwick, Sebastian. "An efficient orientation filter for inertial and inertial / magnetic sensor arrays." (2010).

[24] F. Gustafsson et al., "Particle filters for positioning, navigation, and tracking," in IEEE Transactions on Signal Processing, vol. 50, no. 2, pp. 425-437, Feb. 2002, doi: 10.1109/78.978396.

Aristidis Raptopoulos Chatzistefanou was born in Florina, Greece, in 1996. He received the Diploma degree in electrical and computer engineering from the Aristotle University of Thessaloniki in 2019, where he is currently pursuing the Ph.D. degree, and working as a Research Assistant with the Aristotle University of Thessaloniki. His main research interests include RFID technology, localization and tracking techniques.

Anastasios Tzitzis was born in Thessaloniki, Greece, in 1994. In 2018 he received the Diploma in Electrical and Computer Engineering from Aristotle University of Thessaloniki, where he is currently working toward the Ph.D. degree. At the same time, he is working as a Research and Teaching Assistant at the Aristotle University. His current research interests include analysis and design of antennas, RFID technology and wave propagation.

Spyros Megalou received the MSc degree in Electrical and Computer engineering from the Aristotle University of Thessaloniki, Greece, in 2019, and he is currently pursuing the Ph.D. degree at the same School. His main research interests include RFID technology, localization techniques, microwave applications and antenna design. He is also a member of a space related group (BEAM, Beyond Earth Aristotle Missions) focusing on space experiments and applications.

George Sergiadis received his diploma in Electrical Engineering from the Aristotle University of Thessaloniki, Greece, and his Ph.D. from "Ecole Nationale Supérieure des Télécommunications", in Paris, France.

He is currently full Professor at the Aristotle University of Thessaloniki, Greece, teaching Telecommunications and Biomedical Engineering, since 1985. He has been an August-Wilhelm Scheer visiting professor in TUM, Munich, Germany, a visiting researcher at Media Lab, MIT, also in IBMI, Munich, Germany, and a Distinguished Professor at SIBET, Suzhou, China, for several years.

His current research interests include signal and image processing, and medical imaging.

Antonis G. Dimitriou (S'01-M06-SM'14) received the diploma and the Ph.D. degree in Electrical and Computer Engineering from the Aristotle University of Thessaloniki, Greece, in 2001, and 2006 respectively. Since 2007, he is with the School of Electrical and Computer Engineering of AUTh, where he currently serves as a teaching and research faculty member.

He has participated in more than 20 research projects, 8 of which since 2007 as a principal investigator in the fields of Robotics, RFIDs, and Wireless Sensor Networks. He is currently the coordinator of project "RELIEF", involving continuous RFID inventorying through robotics and project "CUL-TUREID", where RFID equipment will be installed inside the Archaeological Museum of Thessaloniki to monitor RFID tagged exhibits and track visitors. He was a Management Committee Member in the ICT COST Action IC301 "Wireless Power Transmission for Sustainable Electronics (WiPE)". He is the author or co-author of approximately 60 journal and conference papers.

Dr. Dimitriou was the recipient of the Ericsson Award of Excellence in Telecommunications in 2001 and co-recipient of the student-paper award in the 2011 IEEE RFID-TA conference. He received the "IEEE Wireless Communications Letters Exemplary Reviewer" award in 2012 and 2014. He is a Senior IEEE Member since February 2014. He also serves as a reviewer for major journals and as a TPC member for international conferences.